Multilayer Polymer Light-Emitting Diodes: White-Light Emission with High Efficiency**

By *Xiong Gong*,* *Shu Wang*, *Daniel Moses*, *Guillermo C. Bazan*,* and *Alan J. Heeger*

Organic and polymer light-emitting diodes (OLEDs/PLEDs) that emit white light are of interest and potential importance for use in active-matrix displays (with color filters) and because they might eventually be used for solid-state lighting.[1,2] In such applications, the fabrication of large-area devices and the use of low-cost manufacturing technology will be the major issues.[2] The fabrication of PLEDs by processing the active materials from solution (e.g., by using printing technology) promises to be less expensive than that of OLEDs, where deposition of the active layers requires the use of vacuum technology.[2,3] Several approaches have been used to generate white light from OLEDs and PLEDs.[2,4–9] In each case, however, the efficiency was modest and the lifetime was limited by that of the blue emitters. [3,7–12]

White light is characterized by three quantities: The CIE (Commission Internationale d'Eclairage) coordinates, the color temperature (CT), and the color rendering index (CRI).[13] "Pure" white light has CIE coordinates of (0.333, 0.333), and is obtained by balancing the emission of the colors employed. For illumination applications, the CT needs to be equivalent to that of a blackbody source at temperatures between 3000 and 7500 K. The CRI is a numerical measure of how "true" colors look when viewed with the light source. CRI values range from 0 to 100, with 100 representing true color reproduction.

We show that high-performance, multilayer, white-light-emitting PLEDs can be fabricated by using a blend of luminescent semiconducting polymers and organometallic complexes as the emission layer, and water-soluble (or ethanol-soluble) polymers and/or small molecules as the hole-injection/transport layer (HIL/HTL) and the electron injection/transport layer (EIL/ETL). Each layer is spin-cast sequentially from solution. These multilayer PLEDs emit illumination-quality white light with high brightness, high luminous efficiency, suitable CT, stable CIE coordinates, and high CRI.

The device fabrication is described in the Experimental section. The device architecture and the molecular structure of the polymers and small molecules used for fabrication of the devices are shown in Scheme 1. The energy levels of the top of the π-band (highest occupied molecular orbital, HOMO) and the bottom of the π*-band (lowest occupied molecular orbital, LUMO) of PFO-ETM, PVK-SO_3Li, and *t*-Bu-PBD-SO_3Na, and the work functions of Ba and PEDOT:PSS are given in Scheme 2a. The corresponding energy levels of PFO-ETM, Ir(HFP)$_3$, and fluorenone are shown in Scheme 2b.

The selection of materials for the HIL/HTL and EIL/ETL is critical for achieving the band alignment that favors charge injection from the electrodes, for achieving good transport of the respective carriers through the HTL and ETL to the active emission layer, and for hole-blocking (electron-blocking) at the ETL (HTL). PVK-SO_3Li was selected for the HIL/HTL because its HOMO energy level at –5.75 eV is well-aligned with the HOMO energy level of PFO-ETM at –5.80 eV,[14] implying a nearly ohmic contact for hole injection/transport from PVK-SO_3Li to PFO-ETM. *t*-Bu-PBD-SO_3Na was selected for the EIL/ETL because its LUMO at –2.60 eV is only ~0.10 eV higher than the Fermi level of Ba at –2.70 eV (as inferred from the work function). However, even this small electron injection barrier will be reduced by the formation of a dipole layer at the Ba/*t*-Bu-PBD-SO_3Na interface.[12,14,15] Therefore, the combination of good band alignment and carrier blocking achieved by using PVK-SO_3Li for the HIL/HTL and *t*-Bu-PBD-SO_3Na for the EIL/ETL results in sufficiently balanced charge injection/transport to enable high-performance white-light-emitting PLEDs (see Fig. 1). In addition to functioning as the HIL/HTL, the PVK-SO_3Li layer provides a smooth and pinhole-free surface on which the active emission layer can be cast. Moreover, the addition of the HIL/HTL and EIL/ETL to the device architecture leads to significantly reduced leakage currents (from micro-shorts etc.) and thereby significantly reduces the probability of catastrophic shorts.

By using water-soluble (ethanol-soluble) PVK-SO_3Li as the HIL/HTL and *t*-Bu-PBD-SO_3Na as the EIL/ETL, the interfacial mixing problem is solved (the emissive polymer layer is soluble in organic solvents, but not in water). As a result, this

[*] Dr. X. Gong, Prof. G. C. Bazan, Dr. S. Wang, Dr. D. Moses, Prof. A. J. Heeger
Institute for Polymers and Organic Solids
University of California
Santa Barbara, CA 93106 (USA)
E-mail: xgong@physics.ucsb.edu; bazan@chem.ucsb.edu
Prof. G. C. Bazan
Department of Chemistry
University of California
Santa Barbara, CA 93106 (USA)
Dr. S. Wang
Key Laboratory of Organic Solids, Institute of Chemistry
Chinese Academy of Sciences
Beijing 100080 (P.R. China)
Prof. A. J. Heeger
Department of Physics and Materials Department
University of California
Santa Barbara, CA 93106 (USA)

[**] This work was jointly supported by Mitsubishi Chemical Center for Advanced Materials at UC Santa Barbara, by Air Force Office of Scientific Research through the MURI Center ("Polymeric Smart Skins", AFOSRF 49620-01-10364), Program Officer, Dr. Charles Lee. We thank Dr. Gang Yu of Dupont Displays for advice on calculating the CIE coordinates, Dr. Yoshiharu Sato at the Science & Technology Research Center of Mitsubishi Chemical Corporation in Japan for useful discussions, Dr. Steven Xiao at Organic Vision, Inc. (Canada) for providing the conjugated polymers, and Dr. Jack Ostrowski at UC Santa Barbara for synthesis of Ir-complex.

 DOI: 10.1002/adma.200500727

ADVANCED MATERIALS

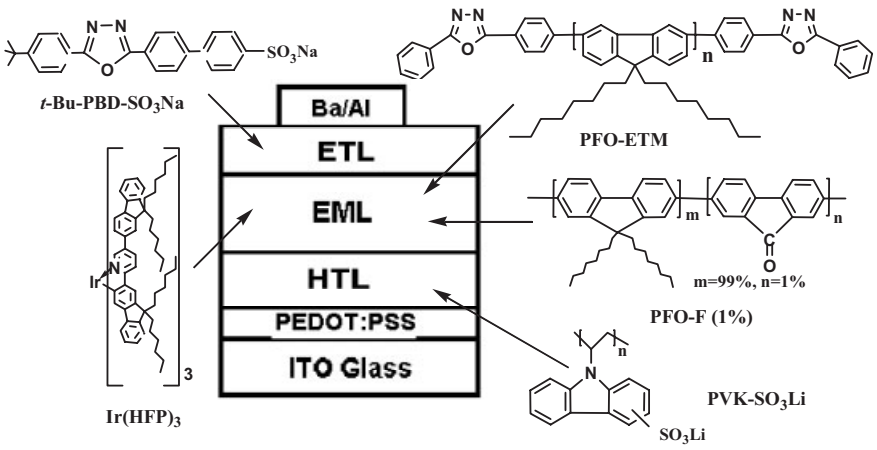

Scheme 1. The device architecture used in this study and the molecular structures of PFO-ETM, PFO-F (1%), $Ir(HFP)_3$, PVK-SO_3Li, and *t*-Bu-PBD-SO_3Na. *t*-Bu-PBD-SO_3Na: 4-(5-(4-*tert*-butylphenyl)-1,3,4-oxadiazole-2-yl)-biphenyl-4′-yl sulfonate sodium salt; PFO-ETM: poly(9,9-dioctylfluorene) end-capped with an electron-transporting moiety, electron-5-biphenyl-1,3,4-oxadiazol; PVK-SO_3Li: poly(vinylcarbazole) sulfonate lithium salt; $Ir(HFP)_3$: tris(2,5-bis-2′-(9′,9′-dihexylfluorene) pyridine) iridium(III); PEDOT: poly(3,4-ethylene dioxythiophene); PSS: poly(styrene sulfonic acid); ITO: indium tin oxide; ETL: electron-transport layer; EML: emissive layer; HTL: hole-transport layer.

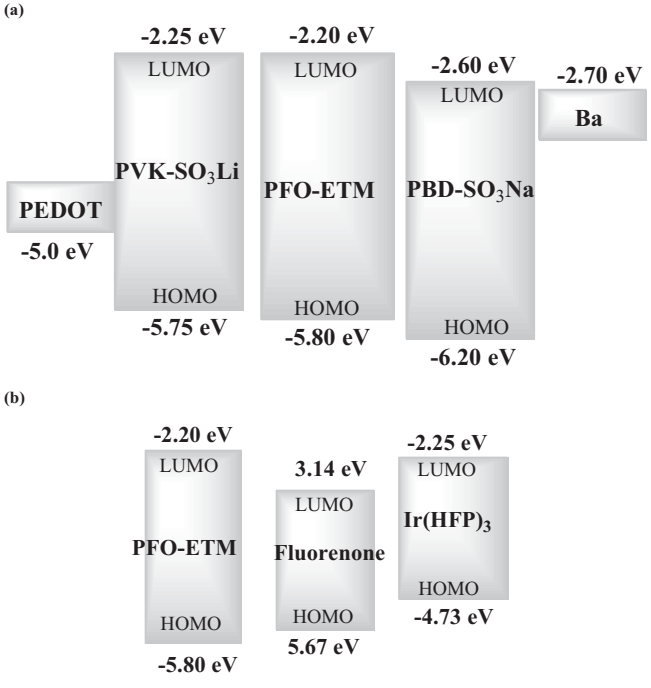

Scheme 2. a) The HOMO and LUMO energy levels of PFO-ETM, PVK-SO_3Li, *t*-Bu-PBD-SO_3Na, and the work functions of PEDOT:PSS and Ba. b) The HOMO and LUMO energy levels of PFO-ETM, PFO-F (1%), and Ir $(HFP)_3$. The shaded areas are the HOMO–LUMO gap; the energies of the top of the π-band (HOMO) and the bottom of the π*-band (LUMO) are indicated in black.

device architecture and process technology can potentially be used for printing large-area multilayer light sources and for other applications in "plastic" electronics.

As specific examples, we have focused on two types of multilayer white-light-emitting PLEDs. Type I devices are fabricated by using PFO-ETM blended with $Ir(HFP)_3$ as the emitter, water-soluble (or ethanol-soluble) PVK-SO_3Li as the HIL/HTL, and *t*-Bu-PBD-SO_3Na as the EIL/ETL. PFO-ETM was selected as the host because more balanced charge carriers can be obtained by end-capping PFO with ETM. Type II devices are fabricated by using blends of PFO-ETM with PFO-F(1%) and $Ir(HFP)_3$ as the emitter, PVK-SO_3Li as the HIL/HTL, and *t*-Bu-PBD-SO_3Na as the EIL/ETL. The luminance (L/cd m^{-2}) versus voltage (V) and current-density (J/mA cm^{-2}) versus V characteristics for type I and type II devices are shown in Figures 2a,b, respectively. Type I devices have a value of $L = 2.4 \times 10^4$ cd m^{-2} at 16 V, and type II devices have a value of $L = 1.0 \times 10^4$ cd m^{-2} at 25 V. The brightness observed from the PLEDs with a HIL/HTL and a EIL/ETL is approximately two times higher than that for those without a HIL/HTL or a EIL/ETL. All devices turn on at approximately 6 V (the turn-on voltage is defined as the voltage at a brightness of 0.1 cd m^{-2}), which is ~1 V higher than that for devices without PVK-SO_3Li, due to the larger film thickness. The reduced turn-on voltage results from the enhancement of the built-in potential in the metal–semiconductor–metal diode by the EIL/ETL.[16]

To evaluate the performance for display applications, a Lambertian intensity profile was assumed; LE_{ext}/cd A^{-1}) and the forward-viewing external power efficiency (PE_{ext}/lm W^{-1}), were measured with the detector subtending a solid angle of only 0.01 sr.[17–20]. LE_{ext} versus J data for devices with PEDOT:PSS as the HIL/HTL, *t*-Bu-PBD-SO_3Na as the EIL/ETL, and devices with PVK-SO_3Li as the HIL/HTL and *t*-Bu-PBD-SO_3Na as the EIL/ETL are shown in Figures 1a,b respectively. The PE_{ext} versus J data for type I and type II devices are also shown in Figures 1a,b. For type I devices, $LE_{ext} = 10.4$ cd A^{-1}, $L = 2391$ cd m^{-2}, and $PE_{ext} = 3$ lm W^{-1} at $J = 23$ mA cm^{-2} ($V = 11$ V). For type II devices, $LE_{ex} = 7.2$ cd A^{-1}, $L = 882$ cd m^{-2}, and $PE_{ext} = 1.5$ lm W^{-1} at $J = 12$ mA cm^{-2} ($V = 15$ V). Note that even at $J = 200$ mA cm^{-2}, type I devices have values of $L = 19500$ cd m^{-2}, $LE_{ext} = 9.5$ cd A^{-1}, and $PE_{ext} = 2$ lm W^{-1}; and type II devices have values of $L = 9600$ cd m^{-2}, $LE_{ext} = 4.8$ cd A^{-1}, and $PE_{ext} = 0.65$ lm W^{-1}. At 200 mA cm^{-2}, LE_{ext} and PE_{ext} are significantly higher than those obtained for any of the white-light-emitting OLEDs and PLEDs reported previously.[3,5–9] Moreover, as shown in Figure 1, the values of LE_{ext} and PE_{ext} obtained from white-light-emitting PLEDs with *t*-Bu-PBD-SO_3Na as the EIL/ETL are higher than those obtained for those without *t*-Bu-PBD-

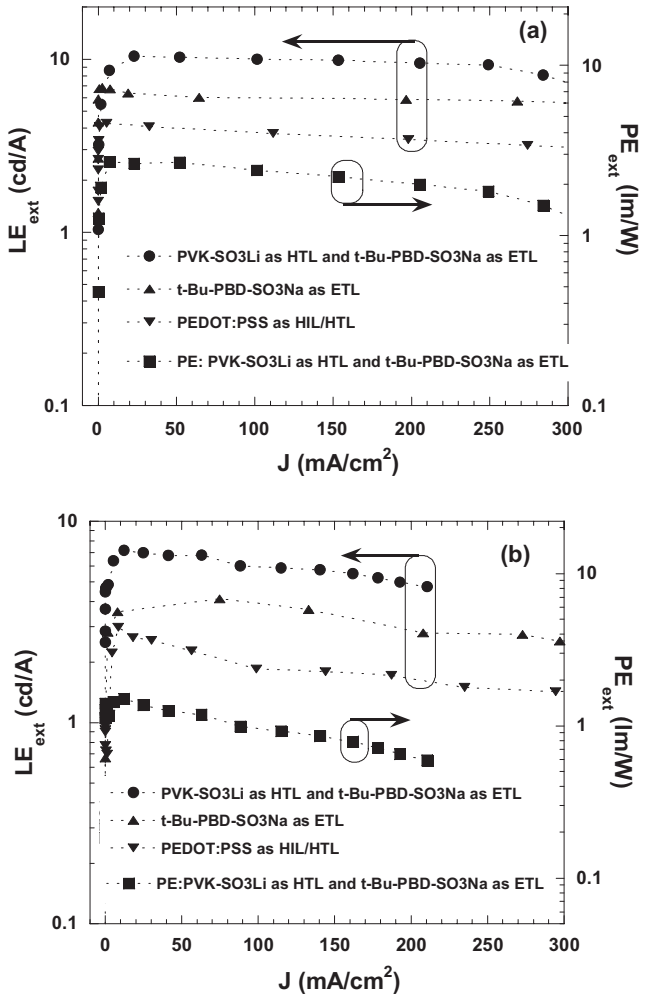

Figure 1. The forward-viewing external luminous efficiency (LE_{ext}, left axis) and external power efficiency (PE_{ext}, right axis) versus current density (J) for a) type I and b) type II devices using the following device configurations: ●, ■: ITO/PEDOT:PSS/PVK-SO_3Li/emissive layer/*t*-Bu-PBD-SO_3Na/Ba/Al; ▲: ITO/PEDOT:PSS/emissive layer/*t*-Bu-PBD-SO_3Na/Ba/Al; ▼: ITO/PEDOT:PSS/emissive layer/Ba/Al.

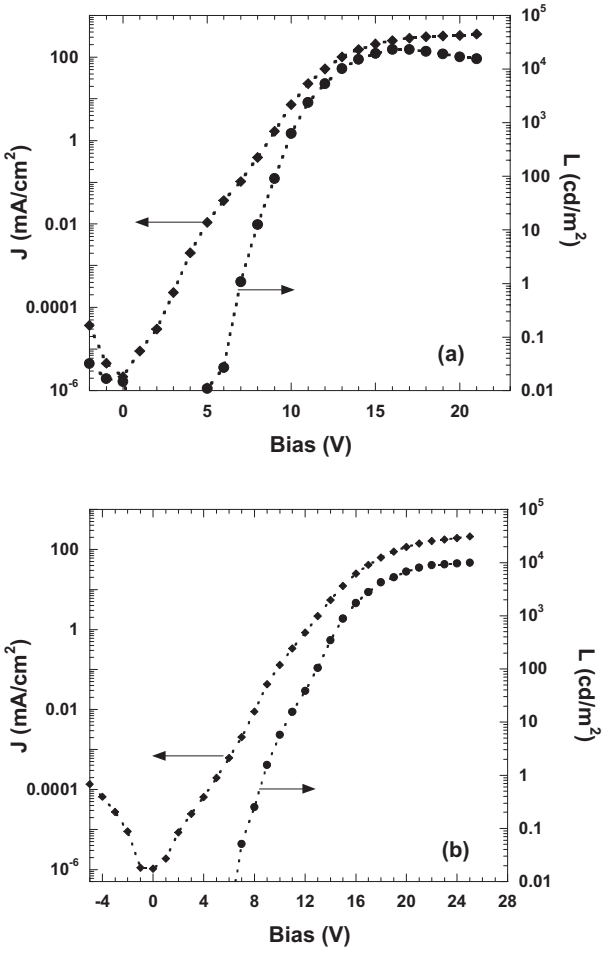

Figure 2. *L* versus voltage and current density versus voltage characteristics for a) type I devices and b) type II devices.

SO_3Na. Similarly, values of LE_{ext} and PE_{ext} for white-light-emitting PLEDs with both PVK-SO_3Na as the HIL/HTL and *t*-Bu-PBD-SO_3Na as the EIL/ETL are higher than that obtained for PLEDs with only *t*-Bu-PBD-SO_3Na as the EIL/ETL.

The improvement in the values of L, LE_{ext}, and PE_{ext} from these white-light-emitting PLEDs can be understood from the energy-level diagrams shown in Scheme 2a. With both a HIL/HTL and a EIL/ETL, the energy barriers for hole and electron injection are eliminated, leading to more balanced injection of holes and electrons. The addition of the HTL and the ETL result in good hole and electron transport from the electrodes to the emissive layer, while simultaneously providing large barriers to the transport of carriers out of the emissive layer prior to radiative recombination. As a result, higher values of L, LE_{ext}, and PE_{ext} are obtained at a given value of J.

In addition, the ETL serves to block the diffusion of metal atoms, such as Ba and Ca, and thereby prevents the generation of quenching centers[21] during the cathode deposition process. In addition, the HTL serves to block indium diffusion into the polymer, a process known to enhance device degradation.[22–24] Both the HTL and the ETL serve to protect the polymer against contamination by oxygen and moisture (exposure to oxygen and water vapor cause degradation of PLEDs).[25,26] Therefore, the stability of multilayer white-light-emitting PLEDs is expected to be better than that of previously reported white-light-emitting PLEDs.[27]

Figures 3a,b show the emission spectra obtained from type I and II devices at different applied voltages. The spectra show the contributions from PFO-ETM, PFO-F (1 %), and $Ir(HFP)_3$.[12,28–30] The mechanism for achieving white light from these PLEDs can be understood in more detail from the energy-level diagrams shown in Scheme 2b. In PLEDs made with $Ir(HFP)_3$:PFO-ETM, the injected holes and electrons can recombine either on the PFO-ETM main chain to produce blue and green emission,[12] or they can be trapped by $Ir(HFP)_3$ with emission of red light from the triplet of

ADVANCED MATERIALS

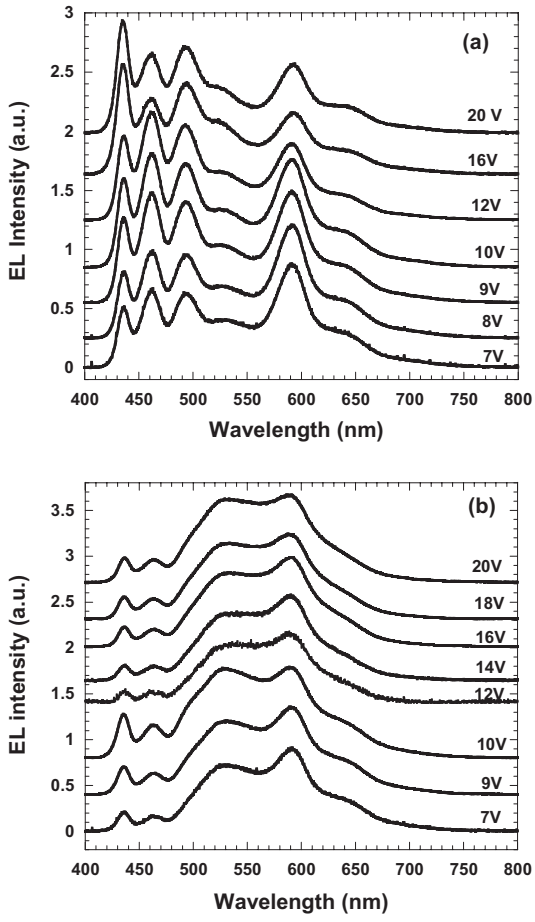

Figure 3. The emission spectra of a) type I devices and b) type II devices at different applied voltages. EL: electroluminescence.

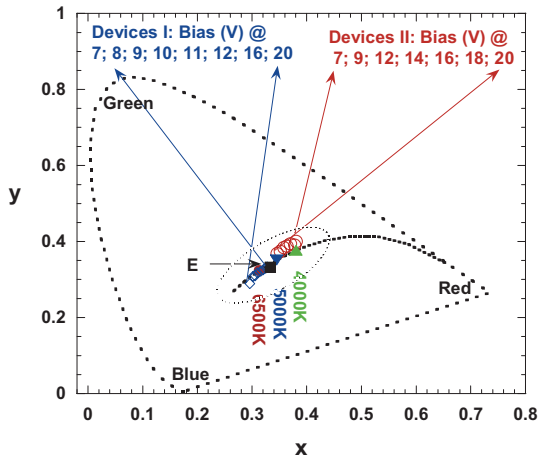

Figure 4. The CIE (1931) chromaticity diagram, with coordinates corresponding to the emission from type I (□) and type II (○) devices biased at different applied voltages. Also shown are the equi-energy point (E) for pure white light (0.333, 0.333) (■) and the coordinates corresponding to color temperatures of 4000 K (▲), 5000 K (▼), and 6500 K (●). The dotted line indicates different color temperatures; the dotted oval indicates the approximate area where the human eye perceives the color as white.

$Ir(HFP)_3$.[28–31] In PLEDs made from the $Ir(HFP)_3$:PFO-F(1 %):PFO-ETM blends, the injected holes and electrons recombine by two processes; direct recombination on the main chain (PFO-ETM) to produce blue and green emission,[12] in parallel with electron and hole trapping on the fluorenone units and on the $Ir(HFP)_3$ followed by radiative recombination with green light from PFO-F (1 %)[28] and red light from the triplet excited state of $Ir(HFP)_3$.[27,29–31]

As demonstrated in Figure 3, the emission spectra are insensitive to the applied voltage, and this occurs even at applied voltages larger than 20 V (not shown). Thus, the quality of white light emitted from these multilayer PLEDs is insensitive to the applied voltage (and current density), and is therefore insensitive to the brightness.

Figure 4 shows the 1931 CIE chromaticity diagram, with coordinates corresponding to the emission from the PLEDs: data points are shown for both type I devices (open squares) and type II devices (open circles) biased at different applied voltages. For type I devices, the CIE coordinates shift from (0.328, 0.334) at $J = 0.10$ mA cm^{-2} to (0.296, 0.290) at $J =$ 334 mA cm^{-2}. For type II devices, the CIE coordinates shift from (0.380, 0.400) at $J = 0.2$ mA cm^{-2} to (0.346, 0.368) at $J = 115$ mA cm^{-2}. All are very close to the CIE coordinates for pure white light, (0.333, 0.333). The stability of the CIE coordinates as a function of applied voltage is much better than those of previously reported white-light-emitting PLEDs/OLEDs.[3,7–9]

Type I devices have a CT value of ~6400 K (which is very close to the CT of average daylight (6500 K)[13]) and a CRI value of 92. Type II devices have a CT value of ~4500 K (which is very close to the CT of sunlight at a solar altitude of 20° (4700 K)[13]) and a CRI value of 86. Both sets of values (CT and CRI) are insensitive to the applied voltage and insensitive to current density and luminance. Therefore, the white light observed from the multilayer PLEDs has stable CIE coordinates, stable CT, and stable CRI values, which are all close to those of "pure" white light.

For solid-state lighting applications, one should include the light emitted through the surface and edge of the glass/ITO substrate when calculating the total efficiency.[32,33] Assuming typical values for the refractive indices of the glass ($n = 1.5$), ITO ($n = 1.8$–2.0), and polymer ($n = 1.6$–1.8), the critical angle, θ, between the direction of the light emitted in the polymer layer and the substrate surface normal is ~36° at the air/polymer interface, and ~62° at the glass/polymer interface.[34–37] Light incident on the interface at an angle greater than the critical angle will be totally internally reflected within the glass/ITO and then waveguided within the device. Although some of the guided light escapes by scattering, the remainder is either partially absorbed within the device or coupled out at the edges of the glass/ITO substrate. Theoretically, the fraction of light emitted in the forward direction is $1/(2n^2)$ of the total, where n is the index of refraction of emitter layer.[37] More detailed optical modeling predicted $3/4n^2$ to be the frac-

tion emitted in the forward direction.[38] Through a series of experiments using an integrating sphere, Cao et al. demonstrated that the measured reduction factor is approximately 2–2.5 times less than the theoretical value, $2n^2 \approx 6$ (assuming $n = 1.7$ for the emitting layer); i.e., closer to $4n^2/3 \approx 3.85$.[39] Forrest and co-workers have obtained similar results; in the small-device approximation, they found that the total LE is larger by a factor of 1.7–2.4 than that observed in the forward-viewing direction.[2,34] Because the luminance was measured in the forward-viewing direction in our experiments (the detector subtended a solid angle of only 0.01 sr[17,19,20,27–31,35]), the total LE (LE_{total}) and total PE (PE_{total}) are larger than the corresponding forward-viewing external LE and PE values by approximately a factor of 2. Thus, for solid-state lighting applications, $LE_{total} = 21$ cd A^{-1} and $PE_{total} = 6$ lm W^{-1} at $J = 23$ mA cm^{-2} for type I devices, and $LE_{total} = 15$ cd A^{-1} and $PE_{total} = 3$ lm W^{-1} at $J = 12$ mA cm^{-2} for type II devices.

In conclusion, we have demonstrated high-efficiency multilayer white-light-emitting PLEDs fabricated with a blend of luminescent semiconducting polymers and organometallic complexes as the emission layer, water-soluble (or ethanol-soluble) PVK-SO_3Li as the HIL/HTL and water-soluble (or ethanol-soluble) *t*-Bu-PBD-SO_3Na as the EIL/ETL. Illumination-quality light is emitted with stable CIE coordinates, stable color temperatures, and stable color rendering indices, all close to those of "pure" white light. More importantly, the promise of producing large areas of high-quality white light with low-cost manufacturing technology make these multilayer white-light-emitting PLEDs attractive for the development of solid-state light sources.

Experimental

The synthesis and characterization of PFO-ETM, PFO-F (1 %), and Ir(HFP)$_3$ have been reported elsewhere [27,28,40].

Synthesis of PVK-SO_3Li: The sulfonation of PVK was performed by the procedure described in the literature [41]. The degree of sulfonation of PVK was about 28 %. The sulfonated PVK was dissolved in a minimum amount of hot ethanol, and the resulting solution was cooled to room temperature. To this solution was added excess EtOLi solution in ethanol and a white precipitate was formed. The precipitate was collected by filtration, washed with cold ethanol, and dried in vacuum to obtain PVK-SO_3Li.

Synthesis of t-Bu-PBD-SO_3Na: 4-(5-(4-*tert*-butylphenyl)-1,3,4-oxadiazole-2-yl)-biphenyl-4′-yl sulfonic acid (*t*-Bu-PBD-SO_3H) was synthesized by the procedure described in the literature [42]. A concentrated solution of *t*-Bu-PBD-SO_3H in water/tetrahydrofuran (6:1 v/v) was added into brine to give a white precipitate. The precipitate was extracted with ethanol and the ethanol was removed to obtain *t*-Bu-PBD-SO_3Na.

Device Fabrication: For device fabrication, we employed poly(3,4-ethylene dioxythiophene): poly(styrene sulfonic acid) (PEDOT:PSS) on indium tin oxide (ITO) as the hole-injecting bilayer electrode. The device structure is (ITO)/PEDOT:PSS/PVK/emissive polymer/PBD/Ba/Al. Patterned ITO-coated glass substrates were cleaned with detergent, distilled water, acetone, and 2-propanol and subsequently in an ultrasonic bath. The substrates were dried in an oven at ~100 °C for 12 h before treatment with UV–ozone. After treatment with UV–ozone for 25 min, a 30 nm layer of PEDOT:PSS was spin-coated onto the substrates, followed by drying on a hotplate at 120 °C for 30 min. The PVK thin film (15 nm) was deposited on top of the PEDOT:PSS by spin-casting from 0.5 wt.-% ethanol solution, followed by drying in a vacuum oven at 100 °C for 24 h (note that the time and temperature for drying the PVK layer can be reduced in a roll-to-roll manufacturing line). A thin film of polymer blend was coated on the top of PVK by spin-casting from toluene solution, followed by baking at 80 °C for 20 min inside a controlled-atmosphere dry box. A PBD thin film (15 nm) was deposited on top of the emissive layer by spin-casting from 0.5 wt.-% ethanol solution, followed by drying inside the glove box at 80 °C for 30 min. The Ba and Al electrodes were thermally deposited through a shadow mask in a vacuum of 1×10^{-7} torr (1 torr ≈ 133 Pa).

Device performance was measured inside the dry box. The current–voltage–luminance characteristics were measured using a Keithley 236 source measurement unit. Electroluminescence (EL) spectra were measured using an Oriel Ocean charge-coupled device (CCD) spectrograph. The luminance was obtained in the forward-viewing direction (detector subtended a 0.01 sr solid angle using a calibrated silicon photodiode). The luminous efficiency was converted from measured luminance [20]. The CIE coordinates, CT, and CRI were quantitatively evaluated from the EL spectra [43,44].

Received: April 9, 2005
Final version: May 3, 2005
Published online: July 12, 2005

[1] a) A. J. Heeger, *Solid State Commun.* **1998**, *107*, 673. b) A. J. Heeger, *Rev. Mod. Phys.* **2001**, *73*, 681.
[2] B. W. D'Andrade, S. R. Forrest, *Adv. Mater.* **2004**, *16*, 1585.
[3] J. Kido, H. Shionoya, K. Nagai, *Appl. Phys. Lett.* **1995**, *67*, 2281.
[4] C. D. Müller, A. Falcou, N. Reckefuss, M. Rojahn, V. Wiederhirn, P. Rudati, H. Frohne, O. Nuyken, H. Becker, K. Meerholz, *Nature* **2003**, *421*, 829.
[5] C. Zhang, A. J. Heeger, *J. Appl. Phys.* **1998**, *84*, 1579.
[6] Z. Shen, P. E. Burrows, V. Bulvic, S. R. Forrest, M. E. Thompson, *Science* **1997**, *276*, 2009.
[7] Y. Hamada, T. Sano, H. Fujii, Y. Nishio, *Jpn. J. Appl. Phys., Part 2* **1996**, *35*, L1339.
[8] Y. Z. Wang, R. G. Sun, F. Meghdadi, G. Leising, A. J. Epstein, *Appl. Phys. Lett.* **1999**, *74*, 3613.
[9] M. Strukelj, R. H. Jordan, A. Dodabalapur, *J. Am. Chem. Soc.* **1996**, *118*, 1213.
[10] U. Scherf, E. J. W. List, *Adv. Mater.* **2002**, *14*, 477.
[11] S. Setayesh, D. Marsitzky, K. Müllen, *Macromolecules* **2000**, *33*, 2016.
[12] X. Gong, P. Iyer, D. Moses, G. C. Bazan, A. J. Heeger, *Adv. Funct. Mater.* **2003**, *13*, 325.
[13] R. W. G. Hunt, *Measuring Color*, 2nd ed., Ellis Horwood, Hemel Hempsted, UK **1991**, pp. 38–109.
[14] A. Rajagopal, C. I. Wu, A. Kahn, *J. Appl. Phys.* **1998**, *83*, 2649.
[15] S. T. Lee, X. Y. Hou, M. G. Mason, C. W. Tang, *Appl. Phys. Lett.* **1998**, *72*, 1593.
[16] Y. Cao, A. J. Heeger, *Adv. Mater.* **1998**, *10*, 917.
[17] *Electroluminescence–From Synthesis to Devices* (Ed: K. Müllen), Wiley-VCH, Weinheim, Germany **2005**, in press.
[18] M. H. Lu, J. C. Sturm, *J. Appl. Phys.* **2002**, *91*, 595.
[19] *Measurement of LEDs*, Commission International de l'Éclariage, Vienna, Austria, **1997**, publication 127.
[20] X. Gong, M. R. Robson, J. C. Ostrowski, D. Moses, G. C. Bazan, A. J. Heeger, *Adv. Mater.* **2002**, *14*, 581.
[21] V. Choong, Y. Park, Y. Gao, T. Wehrmeister, K. Müllen, B. R. Hsieh, C. W. Tang, *Appl. Phys. Lett.* **1996**, *69*, 1492.
[22] M. P. de Jong, L. J. van Ijzendoorn, M. J. A. de Voigt, *Appl. Phys. Lett.* **2000**, *77*, 2255.
[23] G. Greczynski, T. Kugler, W. R. Salaneck, *Thin Solid Films* **1999**, *354*, 129.
[24] J. S. Kim, R. H. Friend, F. Cacialli, *Appl. Phys. Lett.* **1999**, *74*, 3084.

ADVANCED MATERIALS

[25] J. Kim, J. Lee, C. W. Han, N. Y. Lee, I. J. Chung, *Appl. Phys. Lett.* **2003**, *82*, 4238.
[26] P. W. Lom, A. J. Berntsen, C. T. Liedenbaum, H. F. Schoo, Y. V. Croonen, *J. Mater. Sci.: Mater. Electron.* **2000**, *11*, 105.
[27] X. Gong, W. L. Ma, J. C. Ostrowski, G. C. Bazan, D. Moses, A. J. Heeger, *Adv. Mater.* **2004**, *16*, 615.
[28] X. Gong, D. Moses, A. J. Heeger, *Synth. Met.* **2004**, *141*, 17.
[29] X. Gong, J. C. Ostrowski, G. C. Bazan, D. Moses, A. J. Heeger, M. S. Liu, A. K.-Y. Jen, *Adv. Mater.* **2003**, *15*, 45.
[30] X. Gong, W. L. Ma, J. C. Ostrowski, K. Bechgaad, G. C. Bazan, D. Moses, A. J. Heeger, S. Xiao, *Adv. Funct. Mater.* **2004**, *14*, 393.
[31] X. Gong, J. C. Ostrowski, D. Moses, G. C. Bazan, A. J. Heeger, *Appl. Phys. Lett.* **2002**, *81*, 3711.
[32] H. A. E. Keitz, *Light Calculations and Measurements*, 2nd ed., Macmillan, London **1971**.
[33] A. D. Ryer, *Light Measurement Handbook*, International Light Inc., Newburyport, MA **1998**.
[34] B. W. D'Andrade, R. J. Holmes, S. R. Forrest, *Adv. Mater.* **2004**, *16*, 624.
[35] M. H. Lu, J. C. Sturm, *J. Appl. Phys.* **2002**, *91*, 595.
[36] J. Kido, Y. Lizumi, *Appl. Phys. Lett.* **1998**, *73*, 2721.
[37] N. C. Greenham, R. H. Friend, D. D. C. Bradley, *Adv. Mater.* **1994**, *6*, 491.
[38] J. S. Kim, P. H. Ho, N. C. Greenham, R. H. Friend, *J. Appl. Phys.* **2000**, *88*, 1073.
[39] Y. Cao, I. D. Parker, G. Yu, C. Zhang, A. J. Heeger, *Nature* **1999**, *397*, 414.
[40] J. C. Ostrowski, M. R. Robinson, A. J. Heeger, G. C. Bazan, *Chem. Commun.* **2002**, 784.
[41] S. Wang, Z. Zeng, S. Yang, L.-T. Weng, P. C. L. Wong, K. Ho, *Macromolecules* **2000**, *33*, 3232.
[42] T. J. Boyd, R. R. Schrock, *Macromolecules* **1999**, *32*, 6608.
[43] G. Wyszelki, W. S. Stiles, *Color Science*, 2nd ed., Wiley, New York **1982**, pp. 117–232.
[44] D. B. Judd, G. Wyszecki, *Color in Business, Science and Industry*, 3rd ed., Wiley, New York **1975**, pp. 91–388.

Nanoporous Polymer Thin Films via Polyelectrolyte Templating**

By *Qi Li*, *John F. Quinn*, and *Frank Caruso**

Materials containing nanopores are important in a variety of fields, including catalysis,[1,2] separations,[3,4] electronics,[5] optics,[6] and biomaterials engineering.[7,8] Templating techniques represent an effective method for producing such materials (both inorganic and organic) with controlled pore structures. For instance, removable surfactant templates have been used to prepare inorganic mesoporous materials with pore sizes tunable in the range 2–10 nm.[9,10] More recently, it has been demonstrated that a similar approach can be used for the production of mesoporous polymers.[11] Polymer materials with highly ordered pore arrays have also been prepared by exploiting the phase separation of different domains in block copolymers,[12–14] while the possibility of using silica particles as a degradable template has also been demonstrated.[15] Other approaches to preparing nanoporous polymer materials include CO_2 foaming,[16] templating around supramolecular liquid crystals,[17] self-assembly of modified polypeptides,[18] reactive encapsulation of a solvent,[19] and removal of a thermally labile phase.[20] In this paper, we report the use of removable polyelectrolytes in layer-by-layer assembled polyelectrolyte multilayer (PEM) thin films[21,22] as a versatile approach to the production of nanoporous polymer films. The significance of this new method is that, in principle, it can be generalized to any PEM system where two components are fixed and a third can be removed. Further, considering the variety of materials that have been assembled to form PEMs, templates with various molecular conformations may be used to induce well-defined pores or interconnected channels. Since PEMs can be readily transferred from planar to colloidal supports,[23–25] the current approach may also be useful for encapsulating enzymes[26] or drugs[27,28] inside coatings which can be "switched" to give controlled pore architectures.

Many polymer pairs have been used to form PEM films through electrostatic interactions,[29] hydrogen-bonding complexation,[30,31] and other interactions.[32,33] These films are typically prepared by the consecutive deposition of complementary species from single-component solutions onto a solid support. However, recent studies have demonstrated that by having *two* polyelectrolytes in one of the adsorption solutions (i.e., a blend of two polyanions or two polycations), film properties such as thickness, composition, and pH response can be tightly controlled.[34–38] Herein, we demonstrate that by assembling poly(acrylic acid) (PAA) in alternation with a blend of a polyelectrolyte (poly(allylamine hydrochloride), PAH) and a hydrogen-bonding polymer (poly(4-vinylpyridine), P4VP), appropriate precursor films can be prepared for the formation of nanoporous polymer films. Pore formation is achieved by chemically crosslinking the electrostatic component (PAA/PAH) and removing the hydrogen-bonding polymer by increasing the pH (see Scheme 1). Porous PEM thin films have previously been prepared by exploiting polymer rearrangement in the thin films, viz. upon immersing PAA/PAH multilayers in a low-pH solution,[39] or by exposing the PAA/PAH multilayers prepared from salt-containing polyelectrolyte solutions to pure water.[40] The current article represents the first example, to our knowledge, of preparing porous polymer films using a hybrid multilayer-templating approach.

Initial studies were conducted to examine the effect of varying blend-solution composition on the buildup of PAA/(P4VP/PAH) multilayers. These studies were performed using

[*] Prof. F. Caruso, Q. Li, Dr. J. F. Quinn
Centre for Nanoscience and Nanotechnology (CNST)
Department of Chemical and Biomolecular Engineering
The University of Melbourne
Victoria, 3010 (Australia)
E-mail: fcaruso@unimelb.edu.au

[**] This work was supported by the Australian Research Council under the Federation Fellowship and Discovery Project schemes, and by the Victorian State Government under the STI Initiative. We thank A. Yu (CNST) and A. Mariotti (School of Chemistry) for assistance with electrochemistry measurement and analysis.

  DOI: 10.1002/adma.200500666